Chapter

Investigation of Electrochemical Pitting Corrosion by Linear Sweep Voltammetry: A Fast and Robust Approach

Shashanka Rajendrachari

Abstract

Generally, impedance spectroscopy, cyclic voltammetry and polarographic methods are used to study the pitting corrosion of steel, stainless steel and many different alloys. But one can also use linear sweep voltammetry (LSV) to investigate the pitting corrosion phenomenon. LSV is having many advantages over other traditional methods; but more research should take place in this area to foreshorten the lacuna. It is an important electrochemical method that involves solid electrode, fixed potential and fast scan rate. The advantage of using LSV in determining the pitting corrosion is less time required in the order of few seconds, and there is no need of keeping the samples in NaCl or any other electrolytes for many months.

Keywords: linear sweep voltammetry, pitting corrosion, stainless steel, electrolyte, scan rate

1. Introduction

Over the few decades, the use of stainless steel has been increased tremendously in various fields due to its beneficial properties like high corrosion resistance, low thermal expansion, high energy absorption, high strength, good weldability and high toughness [1]. The ferritic stainless steel is composed of a lesser quantity of expensive Ni and 10–20 wt.% of Cr, and it has body-centred cubic (BCC) lattice structure [2]. The properties like high thermal conductivity, low thermal expansion, wear and creep resistance, higher yield strength, excellent high-temperature oxidation resistance and less stress corrosion properties had made the ferritic stainless steel one of the important grades of stainless steel [3]. Some of its applications of ferritic stainless steel are fabricating cold water tank, refrigeration cabinets, bench work, chemical and food processing, water treatment plant, street furniture, electrical cabinets, etc. [4].

However, duplex stainless steel is a combination of equal proportions of austenitic and ferritic stainless steel grades. Ferrite phase imparts high strength, while austenite contributes the toughness and high corrosion resistance [5]. Duplex stainless steel possesses amalgamated properties of both ferritic and austenitic stainless steel, and hence it is one of the popular and widely applicable stainless steels. Duplex

stainless steels have a wide range of applications in various fields like chemical, oil, petrochemical, marine, nuclear power to paper and pulp industries [6–8].

Pitting corrosion is a localised hastened dissolution of metal due to the destruction of the protective passive film on the metal surface. The important steps involved in pitting process are breakdown of the passive film, metastable pitting and pit growth. The mechanism of pitting corrosion involves the dissolution of protective passive film and gradual acidification of the electrolyte caused by its insufficient aeration [9]. This increases the pH of the pits by increasing the anion concentration. Most of the engineering metals and alloys are useful only because of passive films (thickness of nano to micron range) and naturally forming oxide layers on the metal surfaces. This will greatly reduce the rate of corrosion of the metals as well as alloys [10]. But these types of passive films are more often amenable to localised destruction resulting in accelerated dissolution of the underlying metal. This type of localised pitting corrosion results to the accelerated failure of structural components by perforation or pitting or by acting as an initiation site for cracking. Many researchers all over the world published many research papers on pitting corrosion of stainless steel by different electrochemical methods.

Shankar et al. [11] studied pitting corrosion resistance of yttria-dispersed stainless steel by cyclic polarisation experiments in 3.56 wt.% NaCl solution. They concluded that the addition of Y2O3 did not affect the pitting corrosion resistance. Ningshen et al. [12] reported the corrosion resistance of 12 and 15% Cr oxide dispersion strengthened (ODS) steels in 3 and 9 M HNO_3, respectively. They observed that 12% chromium ODS steel exhibits higher corrosion rate than 15% chromium ODS steel at both 3 and 9 M HNO_3 concentrations. Balaji et al. [13] studied the corrosion resistance of yttria aluminium garnet (YAG)-dispersed austenitic stainless steel at different concentrations (1, 2.5 and 7.5 wt.%) of YAG. The corrosion studies were carried out in 0.1 N H_2SO_4 using potentiodynamic polarisation, and they reported that addition of YAG does not increase corrosion rate appreciably, but super-solidus sintering shows higher corrosion resistance than solid-state sintering.

Most of the corrosion studies were carried out using electrochemical methods such as impedance spectroscopy [14], polarographic methods [15], cyclic voltammetry [16], etc. But very limited literature is available so far on the corrosion study of stainless steel samples by linear sweep voltammetry method. Linear sweep voltammetry (LSV) is one of the most important methods of electroanalytical chemistry [17–19], initiated by Heyrovsky. He was honoured with a Nobel Prize in Chemistry in the year 1959 due to his pioneering work on cyclic voltammetry and linear sweep voltammetry. LSV is an important voltammetric method in which the current at a working electrode is measured, while the potential between the working electrode and a reference electrode is swept linearly with time [20]. The Randles-Sevcik theory is mainly based on an assumption of diffusion limitation of the active species in a neutral liquid electrolyte, driven by fast reactions at the working electrode [21–23]. In the case of LSV, a fixed potential range is applied similar to the potential step measurements.

The scan rate (v) is calculated from the slope of the line. We can easily alter the scan rate by changing the time required for sweep. The characteristics of the linear sweep voltammogram mainly depend on the following factors:

- The voltage scan rate
- The rate of the electron transfer reaction
- The chemical reactivity of the electroactive species

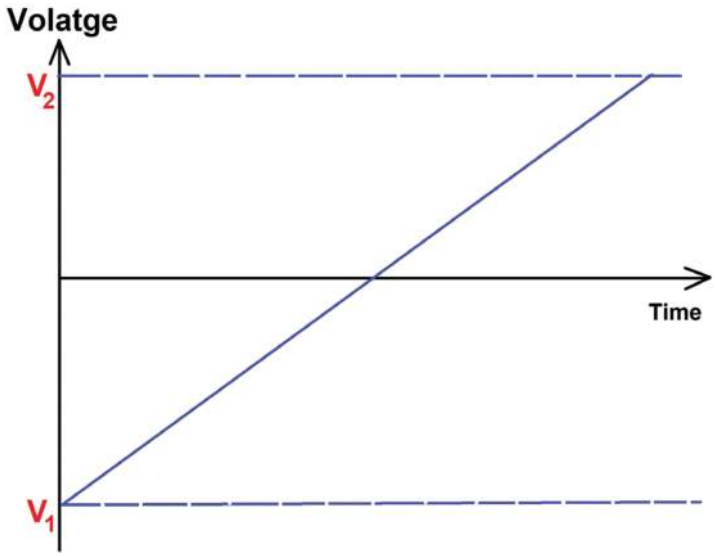

Figure 1.
Linear sweep voltammetry curve [24].

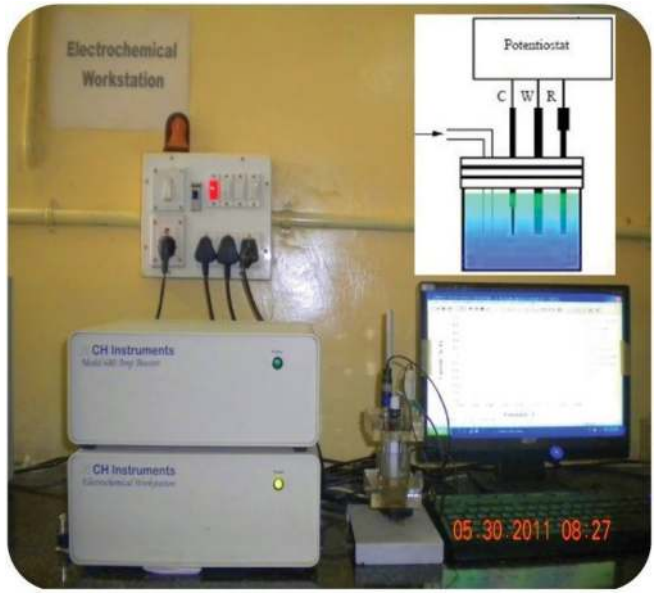

Figure 2.
Linear cyclic voltammetry experimental set-up [25].

But, however, in LSV, the voltage is scanned from a lower limit to an upper limit as depicted below (**Figures 1** and **2**).

This chapter provides an overview of the factors influencing the pitting corrosion of duplex and ferritic stainless steel samples fabricated by spark plasma sintering. The detailed information of fabrication, characterisation and consolidation of duplex and ferritic stainless steels was published by the author in his previous research articles [26–37]. Both the types of stainless steels are used in different fields, and we need to study their corrosion properties before using them as engineering materials. The author has explained the effect of composition, time and different concentrations of electrolytes on the pitting corrosion of duplex and ferritic stainless steels by using LSV.

The experimental data explained in this chapter is performed by the author himself, and part of it is published elsewhere [38, 39]. The corrosion studies were carried out in a well-established three-electrode electrochemical cell using an electrochemical work station CHI-660c model by LSV method. Potential scans were collected in a freely aerated NaCl and H_2SO_4 solutions at room temperature. The experiments were carried out in an electrochemical cell containing Ag/AgCl-saturated KCl as reference electrode and stainless steel samples as working electrode (20 mm diameter) and platinum counter electrode. Corrosion studies were carried out in 0.5, 1 and 2 M concentration of NaCl and H_2SO_4 solutions at different quiet times of 2, 4, 6, 8 and 10 s by LSV method.

2. Mechanism of pitting corrosion in stainless steel

In other words, pitting corrosion is a process of depleting passive layer of the stainless steel aroused by an electrolyte rich in chloride and/or sulphides [25]. **Figure 3** depicts the mechanism of pitting corrosion process in stainless steel. There is a formation of protective Cr_2O_3 passive layer. But in the presence of anions and proper voltage, the passive layer breaks, and the voltage required to deplete the passive layer is called as pitting voltage. After breaking of Cr_2O_3 layer, initiation of pit starts. This increases the anion concentration (Cl^-) in the electrolyte and pit grows further. But in some cases, re-passivation of pit takes place, and this partially improves the corrosion-resistant properties of stainless steel.

Some of the reactions responsible for corrosion in stainless steel at NaCl electrolytes are shown below [38]:

$$\text{Anodic reaction: } Fe \rightarrow Fe^{2+} + 2e^- \text{ (dissolution of iron)}$$

$$Fe^{2+} + 2H_2O \rightarrow FeOH^+ + H_3O^+$$

Formation of $FeOH^+$ is mainly responsible for the sudden increase in current due to the dissolution of Fe metal:

$$\text{Cathodic reaction: } O_2 + 2H_2O + 4e^- \rightarrow 4OH^-$$

$$\text{Main reaction: } Fe^{2+} + 2Cl^- \rightarrow FeCl_2$$

$$FeCl_2 + 2H_2O \rightarrow Fe(OH)_2 + 2HCl$$

Formation of $Fe(OH)_2$ increases the pH of the electrolyte inside a pit from 6 to 2, which induces further corrosion process.

But in the case of H_2SO_4, re-passivation of passive layer takes place due to the following reactions [38]:

$$\text{Anodic reaction:} Fe \rightarrow Fe^{2+} + 2e^- \text{ (dissolution of iron)}$$

$$\text{Cathodic reaction: } 2H^+ + 2e^- \rightarrow H_2$$

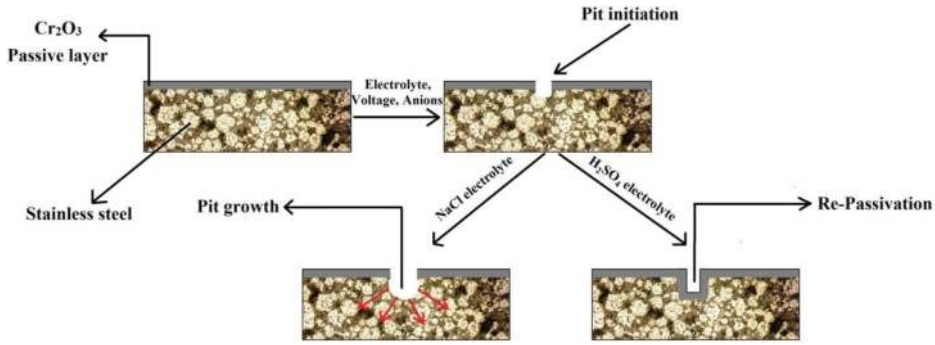

Figure 3.
Mechanism of pitting corrosion in stainless steel samples [38].

The main corrosion reaction gives the products iron sulphate and hydrogen gas as shown below:

$$\text{Main reaction: } Fe + H_2SO_4 \rightarrow FeSO_4 + H_2$$

There is a formation of $FeSO_4$ thin layer on the stainless steel surface, which acts as a passive protective layer for corrosion. But the liberated hydrogen gas scrubs off the $FeSO_4$ layer and causes corrosion [40].

3. A corrosion study of duplex and ferritic stainless steels by LSV

3.1 Different concentrations of NaCl electrolyte solution

We studied the effect of reaction time (quiet time) and different concentrations of NaCl electrolyte on pitting corrosion. The concentrations 0.5, 1 and 2 M of NaCl were prepared in double-distilled water and were used to study the pitting corrosion. The spark plasma-sintered duplex and ferritic stainless steel samples were polished to 4/0 grade finish and cleaned with distilled water before the experiment. The stainless steel whose pitting corrosion properties to be studied was kept inside the electrochemical cell containing NaCl electrolyte, counter electrode and reference electrode. LSV was performed by sweeping a potential from 0.9 to 0 V (adjusted according to the pitting potential) with different quiet times of 2, 4, 6, 8

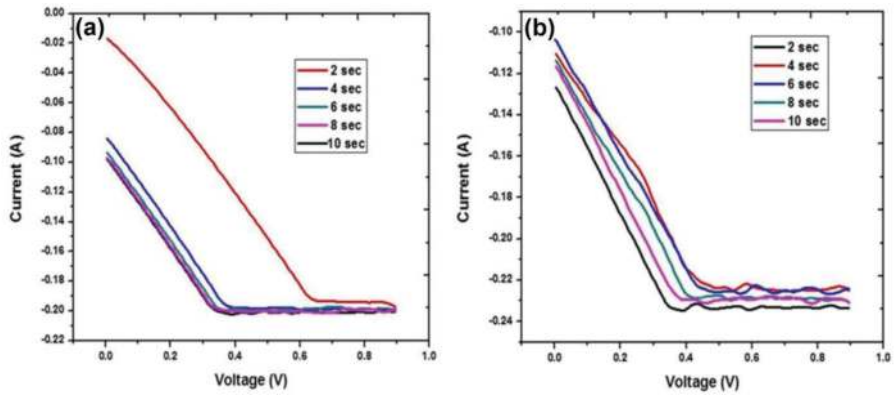

Figure 4.
Potentiometric graphs of (a) duplex stainless steel and (b) ferritic stainless steel, respectively, at 0.5 M NaCl solution [30].

and 10 s. A curve of potential and current was obtained for each individual quiet time at specific concentration. **Figure 4(a)** and **(b)** depicts the LSV curve of current versus voltage variation of duplex and ferritic stainless steel samples at 0.5 M NaCl concentrations in different quiet times.

As the potential sweeps from 0.9 to 0 V, the sharp increase in the current takes place at a particular potential and that potential is called as pitting potential (EP). The sharp increase in the current is due to the availability of more electrons after depleting Cr_2O_3 protective layer. This results in a pit, and it will grow in size if the metal is unprotected and leads to pitting corrosion. EP values of duplex and ferritic stainless steel samples were found to be 0.63 and 0.57 V, respectively. Duplex stainless steel shows more EP value than ferritic stainless steel due to more amount of Cr in duplex than ferritic stainless steel, which imparts maximum strength to interfacial bonding and forms strong oxide layer. Hence, more potential is required to break the oxide layer; the higher the pitting potential, the better is the pitting corrosion resistance [41].

Figure 5(a) and **(b)** shows the current versus voltage graphs of duplex and ferritic stainless steel samples at 1 M NaCl concentration. EP values of duplex and ferritic stainless steel samples are found to be 57 and 0.19 V, respectively. Similarly, **Figure 6(a)** and **(b)** represents the current versus voltage graphs of duplex and ferritic stainless steel samples at 2 M NaCl concentration. The duplex and ferritic stainless steel samples at 2 M NaCl show the EP value of 0.24 and 0.18 V, respectively. From the graphs it is clear that as the concentration of NaCl electrolyte increases from 0.5 to 2 M, then pitting potential of duplex and ferritic stainless steel samples decreases due to the accelerated rate of corrosion reactions at higher concentrations.

3.2 Different concentrations of H_2SO_4 electrolyte solution

The pitting corrosion studies were carried out in a same electrochemical experimental set-up with same experimental condition as the corrosion studies conducted for NaCl electrolyte. But we have used H_2SO_4 here instead of NaCl to study the effect of acid electrolyte on corrosion of duplex and ferritic stainless steel samples. We prepared 0.5, 1 and 2 M concentration of H_2SO_4 electrolyte in double-distilled water and used to study the pitting corrosion of duplex and ferritic stainless steel samples.

A sweep potential of 0.6–0 V (adjusted according to the pitting potential) was applied in LSV with different quiet times of 2, 4, 6, 8 and 10 s, respectively. A voltammetric curve was collected for each individual quiet time at a particular

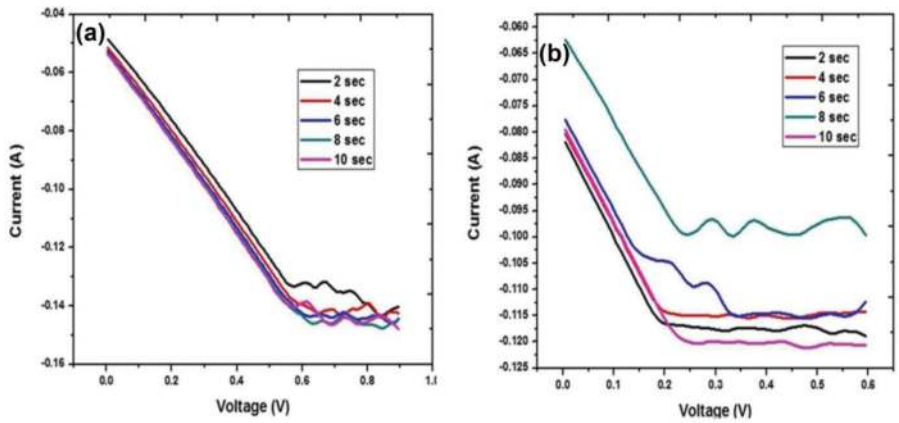

Figure 5.
Potentiometric graphs of (a) duplex stainless steel and (b) ferritic stainless steel, respectively, at 1 M NaCl solution [30].

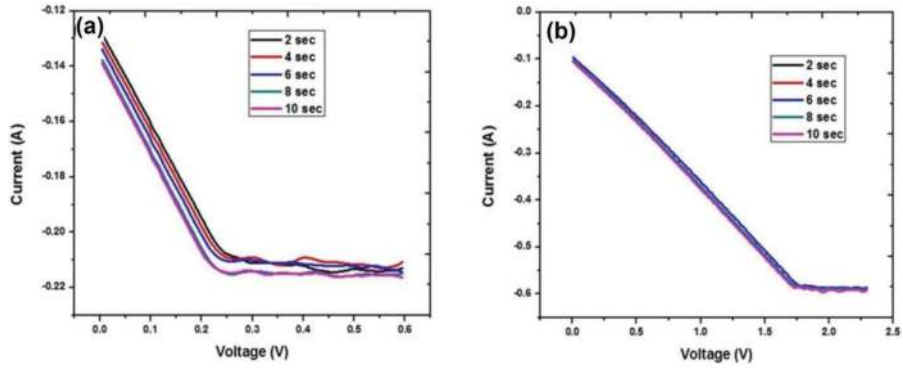

Figure 6.
Potentiometric graphs of (a) duplex stainless steel and (b) ferritic stainless steel, respectively, at 2 M NaCl solution [30].

constant concentration. LSV curve of current versus voltage variation in duplex and ferritic stainless steel samples at 0.5 M H_2SO_4 electrolyte after 2, 4, 6, 8 and 10 s are shown in **Figure 7(a)** and **(b)**, respectively. There is a sharp and sudden increase in the current between the potential 0.6–0 V similar to NaCl electrolyte. EP values of duplex and ferritic stainless steel samples are found to be 0.18 and 0.14 V, respectively.

We also studied the effect of EP at 1 and 2 M H_2SO_4 concentrations by maintaining the same procedure as explained above. **Figure 8(a)** and **(b)** represents the current versus voltage graphs of duplex and ferritic stainless steel samples at 1 M H_2SO_4 solution. EP values of duplex and ferritic stainless steel samples were found to be 0.17 and 0.14 V, respectively.

Similarly, **Figure 9(a)** and **(b)** shows the current versus voltage graphs of duplex and ferritic stainless steel samples at 2 M H_2SO_4 solution. Duplex and ferritic stainless steel samples have an EP value of 0.028 and −0.013 V, respectively, as shown in **Figure 9**.

In the pitting corrosion study during 0.5 and 1 M H_2SO_4 electrolyte, the formed protective $FeSO_4$ layer bounds strongly to the surface of both the stainless steels along with Cr_2O_3 passive layer, and hence hydrogen gas liberated during these concentrations is not enough to break the oxide layer to form a pit and to initiate corrosion. The pitting corrosion studies at 0.5 and 1 M H_2SO_4 solution concluded with higher pitting potential. But with 2 M H_2SO_4 solution, the pitting potential is very low, as the hydrogen gas liberated is sufficient to scrub off the formed $FeSO_4$

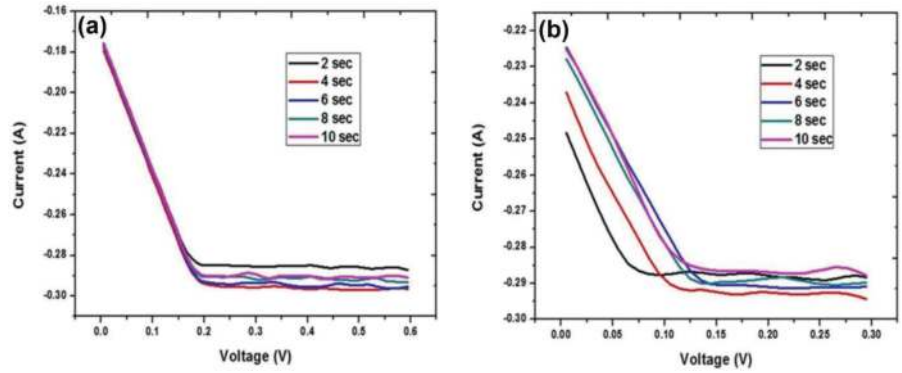

Figure 7.
Potentiometric graphs of (a) duplex stainless steel and (b) ferritic stainless steel, respectively, at 0.5 M H_2SO_4 solution [30].

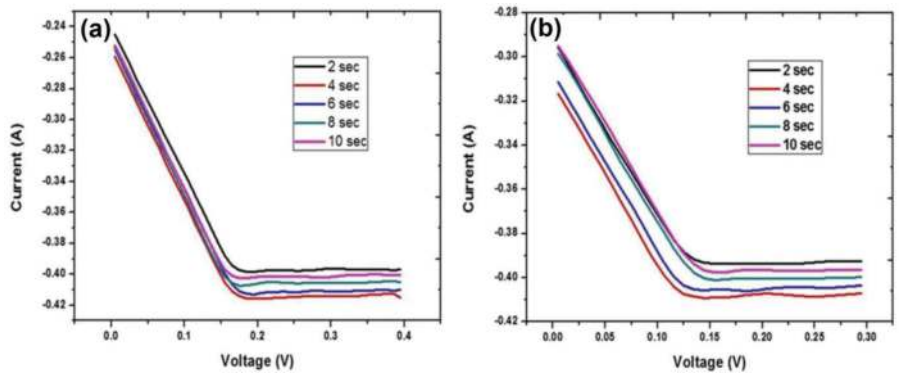

Figure 8.
Potentiometric graphs of (a) duplex stainless steel and (b) ferritic stainless steel, respectively, at 1 M H_2SO_4 solution [30].

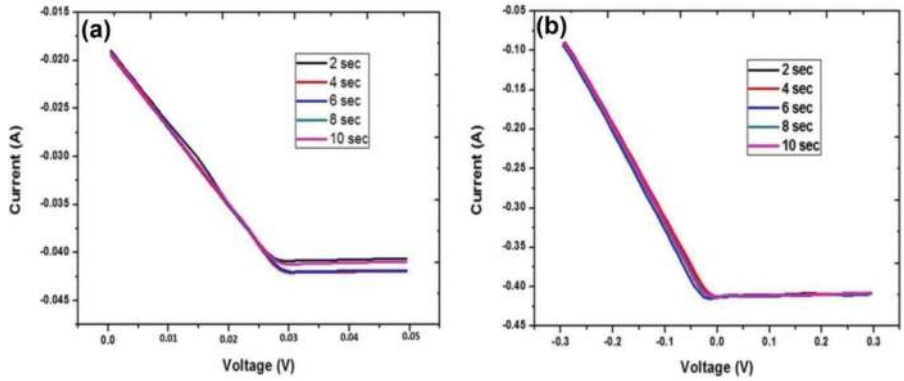

Figure 9.
Potentiometric graphs of (a) duplex stainless steel and (b) ferritic stainless steel, respectively, at 2 M H_2SO_4 solution [30].

Type of stainless steel	Concentration of the electrolyte (M)	Pitting potential (E_P) in NaCl	Pitting potential (E_P) in H_2SO_4
Duplex stainless steel	0.5	0.63	0.18
	1	0.57	0.16
	2	0.24	0.02
Ferritic stainless steel	0.5	0.57	0.14
	1	0.19	0.14
	2	0.18	−0.01

Table 1.
The EP values of duplex and ferritic stainless steels at NaCl and H_2SO_4 solutions.

layer at very low potential. As a result of this, both the stainless steel samples show low pitting potential at 2 M H_2SO_4.

Pitting potential value obtained for H_2SO_4 electrolyte is very low compared to the results obtained for NaCl electrolyte; therefore, duplex and ferritic stainless steel samples undergo corrosion easily in the presence of H_2SO_4 compared to NaCl electrolyte. The values of EP and current density with different electrolytes were tabulated in **Table 1**.

4. Post-corrosion microstructural analysis

Field emission scanning electron microscope (FESEM) images of duplex and ferritic stainless steel samples are shown in **Figure 10**. The grey-coloured regions in the FESEM images are due to pitting corrosion.

To study the further characteristics of pitting corrosion, we have used optical microscope. The optical image analysis was performed to investigate the microstructure of pitting-corroded duplex and ferritic stainless steels. **Figures 11** and **12** show the microstructure and phase analysis of duplex and ferritic stainless steels after pitting corrosion. As both the stainless steel samples were consolidated by spark plasma sintering method at 1000°C, we can see very less porosity ratios. The black-coloured region in **Figure 11** is pitting-corroded region containing iron oxide. Both the stainless steel samples are having black-coloured region in the microstructure, confirming the pitting corrosion process during electrochemical measurement. All the microstructural analysis was performed to only the stainless steel samples whose corrosion studies were conducted by LSV method at 2 M H_2SO_4 solution.

According to corrosion studies, the rate of corrosion is more in ferritic stainless steel than duplex stainless steel, and it was also confirmed by microstructural analysis.

Phase analysis was carried out to study the volume fraction of iron oxide present in both the stainless steel samples. The presence of iron oxide volume percentage is more in ferritic stainless steel than in duplex stainless steel samples. The volume fraction of iron oxide phase is determined by AxioVision Release software attached to an optical microscope. In **Figure 12**, the red-coloured region corresponds to corroded (iron oxide) stainless steel part, and green colour corresponds to uncorroded stainless steel.

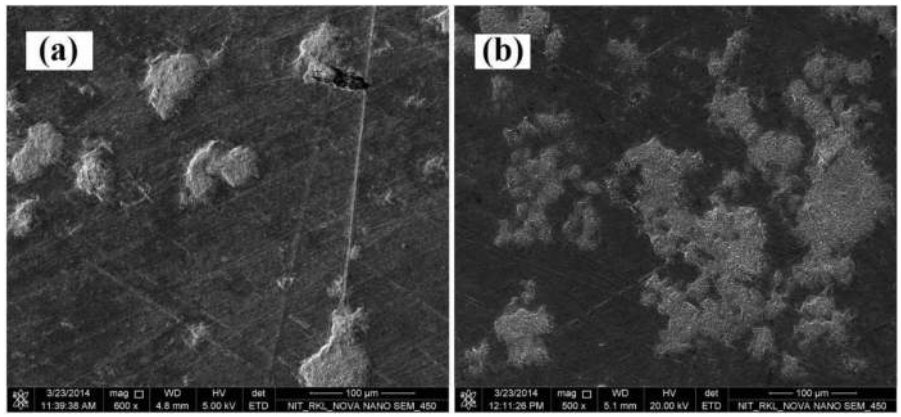

Figure 10.
FESEM images of (a) duplex stainless steel and (b) ferritic stainless steel [30].

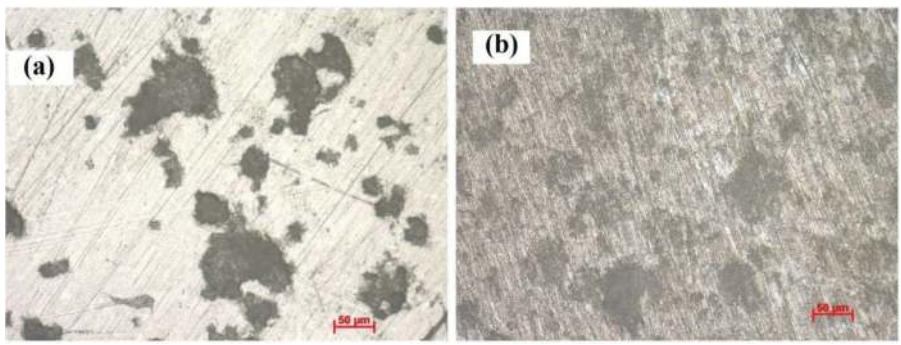

Figure 11.
Optical microscope images of (a) duplex stainless steel and (b) ferritic stainless steel [30].

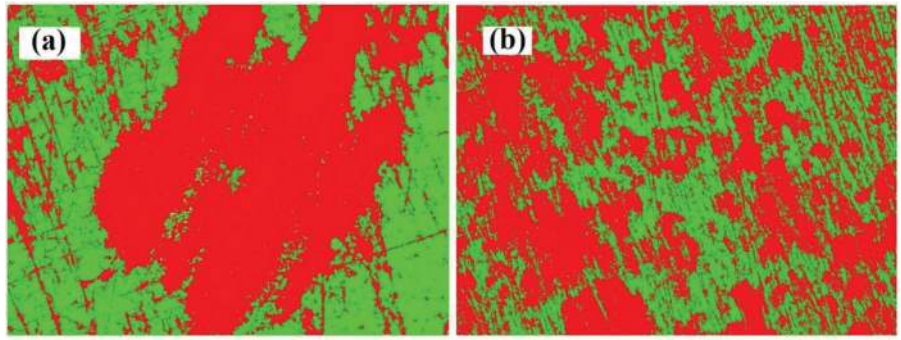

Figure 12.
Optical image phase analysis of (a) duplex stainless steel and (b) ferritic stainless steel using AxioVision Release software (similar to **Figure 11***, all the images are in a magnification of 50 μm scale bars) [30].*

5. Conclusion of the chapter

In the present chapter, we discussed the pitting corrosion properties of SPS-consolidated stainless steel samples by LSV method at different concentrations of NaCl and H_2SO_4 solutions. As the concentration of both the electrolytes increases from 0.5 to 2 M, then pitting potential of duplex and ferritic stainless steels started to decrease due to the accelerated rate of corrosion reactions at higher concentrations. Microstructural analysis by FESEM and optical microscope shows corroded regions of stainless steel samples. The presence of iron oxide volume percentage is more in ferritic stainless steel than in duplex stainless steel samples. The mechanism of pitting corrosion in H_2SO_4 and NaCl solutions is almost the same; but the only difference is the extent of pitting, pitting potential and pitting current values. Pitting potential value obtained for H_2SO_4 electrolyte is comparatively low compared to the results obtained for NaCl electrolyte. From the results, we can conclude that duplex and ferritic stainless steel samples undergo corrosion easily in the presence of H_2SO_4 than NaCl electrolyte.

Nomenclature

wt.%	weight percentage
MPa	megapascal
°C	degree in celsius
nm	nanometre
μm	micrometre
IP	pitting current
EP	pitting potential
V	voltage
J	current density
M	molar
A	ampere
ip	peak current
A	area of electrode
D	diffusion coefficient
Co	concentration
υ	scan rate

DOI: http://dx.doi.org/10.5772/intechopen.80980

Author details

Shashanka Rajendrachari
Department of Metallurgical and Materials Engineering, Bartin University, Bartin, Turkey

*Address all correspondence to: shashankaic@gmail.com

References

[1] Philip Selvaraj D, Chandramohan P, Mohanraj M. Optimization of surface roughness, cutting force and tool wear of nitrogen alloyed duplex stainless steel in a dry turning process using Taguchi method. Measurement. 2014;**49**:205-215

[2] AK Steel Stainless Steels Corporate Headquarters. AK Steel Corporation 9227 Centre Pointe Drive West Chester, Ohio 45069, (513) 425-5000

[3] Kurzydłowski KJ. Microstructural refinement and properties of metals processed by severe plastic deformation. Bulletin of the Polish Academy of Sciences Technical Sciences. 2004;**52**:275

[4] AustralWright Metals. Stainless Steel—Properties and Applications of Ferritic Grade Stainless Steel. Australia: Austral Wright Metals; 2008

[5] Dobrzanski LA, Brytan Z, Actis Grande M, Rosso M. Properties of duplex stainless steels made by powder metallurgy. Archives of Materials Science and Engineering. 2007;**28**:217-223

[6] Herenu S, Alvarez-Armas I, Armas AF. The influence of dynamic strain ageing on the low cycle fatigue of duplex stainless steel. Scripta Materialia. 2001;**45**:739-745

[7] Miyamoto H, Mirnaki T, Hashimoto S. Super plastic deformation of microspecimens of duplex stainless steel. Materials Science and Engineering A. 2001;**319**:779-783

[8] Schofield MJ, Bradsha R, Cottis RA. Stress corrosion cracking of duplex stainless steel weldments in sour conditions. Materials Performance. 2009;**35**:65-70

[9] Yuan Ma F. Corrosive effects of chlorides on metals. In: Bensalah N, editor. Pitting Corrosion. China: In Tech; 2012. ISBN: 978-953-51-0275-5.

[10] Frankel GS. Pitting corrosion of metals: A review of the critical factors. Journal of the Electrochemical Society. 1998;**145**:2186-2198

[11] Shankar J, Upadhyaya A, Balasubramaniam R. Electrochemical behavior of sintered oxide dispersion strengthened stainless steels. Corrosion Science. 2004;**46**:487-498

[12] Ningshen S, Sakairi M, Suzuki K, Ukai S. The corrosion resistance and passive film compositions of 12% Cr and 15% Cr oxide dispersion strengthened steels in nitric acid media. Corrosion Science. 2014;**78**:322-334

[13] Balaji S, Upadhyaya A. Electrochemical behavior of sintered YAG dispersed 316L stainless steel composites. Materials Chemistry and Physics. 2007;**101**:310-316

[14] Chen J, Matthew Asmussen R, Zagidulin D, Noel JJ, Shoesmith DW. Electrochemical and corrosion behavior of a 304 stainlesssteel-based metal alloy waste form in dilute aqueous environments. Corrosion Science. 2013;**66**:142-152

[15] Li CX, Bell T. Corrosion properties of plasma nitrided AISI 410 martensitic stainless steel in 3.5% NaCl and 1% HCl aqueous solutions. Corrosion Science. 2006;**48**:2036-2049

[16] Metikos-Hukovic M, Babic R, Grubac Z, Petrovic Z, Lajci N. High corrosion resistance of austenitic stainless steel alloyed with nitrogen in an acid solution. Corrosion Science. 2011;**53**:2176-2183

[17] Bard AJ, Faulkner LR. Electrochemical Methods:

Fundamentals and Applications. New York: John Wiley & Sons; 2001

[18] Yan D, Bazant MZ, Biesheuvel PM, Pugh MC, Dawson FP. Theory of linear sweep voltammetry with diffuse charge: Unsupported electrolytes, thin films, and leaky membranes. Physical Review E. 2017;**95**:033303

[19] Compton RG, Laborda E, Ward KR. Understanding Voltammetry: Simulation of Electrode Processes. London: Imperial College Press; 2014

[20] Nahir TM, Clark RA, Bowden EF. Linear-sweep voltammetry of irreversible electron transfer in surface-confined species using the Marcus theory. Analytical Chemistry. 2002;**66**:2595-2598

[21] Randles JEB. Kinetics of rapid electrode reactions. Discussions of the Faraday Society. 1947;**1**:11

[22] Randles JEB. A cathode ray polarograph. Part II.—The current-voltage curves. Transactions of the Faraday Society. 1948;**44**:327

[23] Collect SA. Oscillographic polarography with periodical triangular voltage. Czechoslovak Chemical Communications. 1948;**13**:349-377

[24] Linear Sweep and Cyclic Voltammetry: The Principles. Department of Chemical Engineering and Biotechnology. Available from: https://www.ceb.cam.ac.uk/research/groups/rg-eme/teaching-notes/linear-sweep-and-cyclic-voltametry-the-principles

[25] Shashanka R. Fabrication of nano-structured duplex and ferritic stainless steel by planetary milling followed by consolidation [PhD thesis]. India: NIT Rourkela; 2016

[26] Shashanka R, Chaira D. Phase transformation and microstructure study of nano-structured austenitic and ferritic stainless steel powders prepared by planetary milling. Powder Technology. 2014;**259**:125-136

[27] Shashanka R, Chaira D. Development of nano-structured duplex and ferritic stainless steel by pulverisette planetary milling followed by pressureless sintering. Materials Characterization. 2015;**99**:220-229

[28] Shashanka R, Chaira D. Optimization of milling parameters for the synthesis of nano-structured duplex and ferritic stainless steel powders by high energy planetary milling. Powder Technology. 2015;**278**:35-45

[29] Shashanka R, Chaira D, Kumara Swamy BE. Electrocatalytic response of duplex and yttria dispersed duplex stainless steel modified carbon paste electrode in detecting folic acid using cyclic voltammetry. International Journal of Electrochemical Science. 2015;**10**:5586-5598

[30] Shashanka R, Chaira D, Kumara Swamy BE. Electrochemical investigation of duplex stainless steel at carbon paste electrode and its application to the detection of dopamine, ascorbic and uric acid. International Journal of Scientific & Engineering Research. 2015;**6**:1863-1871

[31] Gupta S, Shashanka R, Chaira D. Synthesis of nano-structured duplex and ferritic stainless steel powders by planetary milling: An experimental and simulation study. 4th National Conference on Processing and Characterization of Materials. IOP Conference Series: Materials Science and Engineering. 2015;**75**:012033

[32] Shashanka R, Chaira D. Effects of nano-Y_2O_3 and sintering parameters on the fabrication of PM duplex and ferritic stainless steels. Acta Metallurgica Sinica (English Letters). 2016;**29**:58-71

[33] Nayak AK, Shashanka R, Chaira D. Effect of nanosize yttria and tungsten addition to duplex stainless steel during high energy planetary milling. 5th National Conference on Processing and Characterization of Materials. IOP Conference Series: Materials Science and Engineering. 2016;**115**. DOI: 012008

[34] Shashanka R, Chaira D, Kumara Swamy BE. Fabrication of yttria dispersed duplex stainless steel electrode to determine dopamine, ascorbic and uric acid electrochemically by using cyclic voltammetry. International Journal of Scientific & Engineering Research. 2016;**7**:1275-1285

[35] Shashanka R, Chaira D. Effect of sintering temperature and atmosphere on non-lubricated sliding wear of nano-yttria dispersed and yttria free duplex and ferritic stainless steel fabricated by powder metallurgy. Tribology Transactions. 2017;**60**:324-336

[36] Shashanka R, Chaira D, Chakravarty D. Fabrication of nano-yttria dispersed duplex and ferritic stainless steels by planetary milling followed by spark plasma sintering and non-lubricated sliding wear behaviour study. Journal of Materials Science and Engineering B. 2016;**6**:111-125

[37] Shashanka R. Synthesis of nano-structured stainless steel powder by mechanical alloying—An overview. International Journal of Scientific & Engineering Research. 2017;**8**:588-594

[38] Shashanka R, Chaira D, Kumara Swamy BE. Effect of Y_2O_3 nanoparticles on corrosion study of spark plasma sintered duplex and ferritic stainless steel samples by linear sweep voltammetric method. Archives of Metallurgy and Materials. 2018;**63**:745-759

[39] Shashanka R. Effect of sintering temperature on the pitting corrosion of ball milled duplex stainless steel by using linear sweep voltammetry. Analytical & Bioanalytical Electrochemistry. 2018;**10**:349-361

[40] Sulphuric Acid on the Web. Knowledge for the Sulphuric Acid Industry. DKL Engineering, Inc. Corrosion. June 6, 2005

[41] Tamarit EB, García-Garcia DM, Garcia Anton J. Imposed potential measurements to evaluate the pitting corrosion resistance and the galvanic behaviour of a highly alloyed austenitic stainless steel and its weldment in a LiBr solution at temperatures upto 150°C. Corrosion Science. 2011;**53**:784